LIQUID CRYSTALS

Shaping colloidal bananas to reveal biaxial, splay-bend nematic, and smectic phases

Carla Fernández-Rico[1], Massimiliano Chiappini[2], Taiki Yanagishima[1], Heidi de Sousa[1], Dirk G. A. L. Aarts[1], Marjolein Dijkstra[2], Roel P. A. Dullens[1]*

Understanding the impact of curvature on the self-assembly of elongated microscopic building blocks, such as molecules and proteins, is key to engineering functional materials with predesigned structure. We develop model "banana-shaped" colloidal particles with tunable dimensions and curvature, whose structure and dynamics are accessible at the particle level. By heating initially straight rods made of SU-8 photoresist, we induce a controllable shape deformation that causes the rods to buckle into banana-shaped particles. We elucidate the phase behavior of differently curved colloidal bananas using confocal microscopy. Although highly curved bananas only form isotropic phases, less curved bananas exhibit very rich phase behavior, including biaxial nematic phases, polar and antipolar smectic-like phases, and even the long-predicted, elusive splay-bend nematic phase.

Curvature has an enormous impact on the functionality and self-assembly of elongated microscopic building blocks (*1*, *2*). In the biological world, for instance, curved, rod–shaped bacteria outperform their straight counterparts in surface-colonization and swimming efficiency, which makes them ubiquitous in marine environments (*3*, *4*). Many cellular functions, such as cell division or endocytosis, rely on the ability of "banana-shaped" proteins to generate curvature in cell membranes (*5*, *6*). Curvature is also of key importance at the molecular scale where, for example, banana-shaped or bent-core molecules exhibit a fascinating range of new liquid crystalline phases with distinctive features such as supramolecular chirality and polarity (*7*–*9*). This has led to a surge of interest in banana-shaped liquid crystals from both a fundamental and technological point of view. They are not only ideal systems to study, for example, the spontaneous chiral symmetry breaking in systems of achiral molecules (*10*–*13*) but also excellent candidates for achieving faster switching speeds in display technologies (*14*, *15*).

Over the past two decades, more than 50 new banana-shaped liquid crystalline phases have been reported, depending primarily on the molecular curvature (*7*–*9*). The vast majority of these are smectic (Sm) phases, because the curved shape of the constituting molecules promotes their locking into smectic layers (*8*, *9*). The large stability of Sm phases has also been observed in experiments of colloidal "boomerang-like" particles (*16*) and in computer simulations of similarly shaped particles (*17*). The rather uncommon observation of nematic phases in banana-shaped systems (*18*, *19*) has been of interest for the past 20 years, not least because of their potential to form chiral and biaxial nematic phases (*13*, *17*, *20*, *21*). Examples of chiral and biaxial nematic phases are the twist-bend (N_{TB}) and the splay-bend (N_{SB}) nematic phases, respectively, in both of which the particle orientation is modulated in space. Whereas in the N_{TB} phase the particles exhibit a periodic twist in space resulting in a chiral phase, the N_{SB} phase exhibits periodic splay and bend modulations of the particle orientation in a single plane, thus showing biaxiality but not chirality (*12*).

The N_{TB} and N_{SB} phases were postulated more than 40 years ago by Meyer (*22*), and later independently by Dozov (*12*), who suggested that bend deformations in the orientation field of banana-shaped particles should be accompanied either by twist or splay deformations to fill three-dimensional (3D) space. Whereas the N_{TB} phase has been observed in thermotropic liquid crystals [see, e.g., (*23*–*25*)], the existence of the N_{SB} phase has yet to be confirmed experimentally. Computer simulations suggested that the N_{SB} phase can be found in systems of hard boomerangs—that is, rod-like particles with a sharp kink—if the Sm phase is destabilized by polydispersity in the particle length or by smooth curvature in the particle shape (*17*). Experimentally studying the impact of features such as the curvature on the structure of banana-shaped systems at the particle level is thus crucial for a deeper understanding of the formation and properties of these phases. However, banana-shaped liquid crystals are typically characterized using birefringence and x-ray diffraction techniques, where direct information about structural details is not available at the molecular scale. This prompts the need for a colloidal analog, where such microscopic structural information is readily accessible using optical microscopy. However, despite the abundance of liquid crystal–forming colloidal particles such as rods, boomerangs, and platelets (*26*–*28*), there is no system of smoothly curved colloidal rods available. As such, the rich phase behavior predicted for banana-shaped particles has yet to be experimentally uncovered at the particle level.

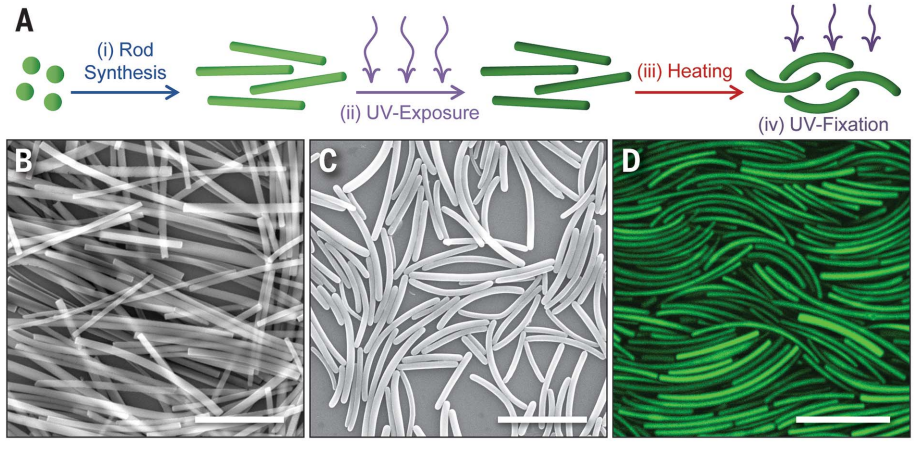

Fig. 1. Synthesis of colloidal SU-8 banana-shaped particles. (**A**) Schematic showing the synthesis of SU-8 banana-shaped particles. In the first step, straight SU-8 rods are synthesized by shearing an emulsion of SU-8 droplets (*29*, *30*). In the second step, the rods are partially cross-linked through exposure to UV light. In the third step, the partially cross-linked rods are heated to induce a shape deformation into banana-shaped particles, before they are UV-cured in the fourth step. (**B** and **C**) Scanning electron microscopy images of (B) the rods obtained after the synthesis with no heating and (C) the colloidal SU-8 bananas (t_{UV} = 45 min) obtained with heating. (**D**) Confocal microscopy image of the fluorescent colloidal SU-8 bananas. Scale bars are 10 μm.

[1]Department of Chemistry, Physical and Theoretical Chemistry Laboratory, University of Oxford, South Parks Road, Oxford OX1 3QZ, UK. [2]Soft Condensed Matter, Debye Institute for Nanomaterials Science, Department of Physics, Utrecht University, Princetonplein 1, 3584 CC Utrecht, Netherlands.
*Corresponding author. Email: roel.dullens@chem.ox.ac.uk

In this work, we develop a method to produce, in bulk, fluorescent curved colloidal rods—colloidal bananas—with tunable dimensions and curvature. Our method relies on the temperature-driven buckling of initially straight rods made of SU-8 photoresist into colloidal bananas. The extent of the shape deformation, and hence the final curvature of the particles, is controlled by the rigidity of the SU-8 rods during the heating. Using confocal microscopy, we elucidate the phase behavior of three differently curved banana-shaped particles at the single-particle level. Although isotropic phases are found for highly curved bananas, very rich phase behavior—including biaxial nematic, splay-bend nematic, and polar and antipolar smectic-like structures—is observed for less curved bananas.

Shaping colloidal SU-8 particles: From rods to banana-shaped particles

Our method to produce colloidal SU-8 banana-shaped particles consists of four main steps, which are illustrated in Fig. 1A: (i) synthesis of rods, (ii) ultraviolet (UV) exposure, (iii) heating, and (iv) UV curing. In the first step, polydisperse straight SU-8 rods of ~20 μm in length (Fig. 1B) are synthesized by vigorously

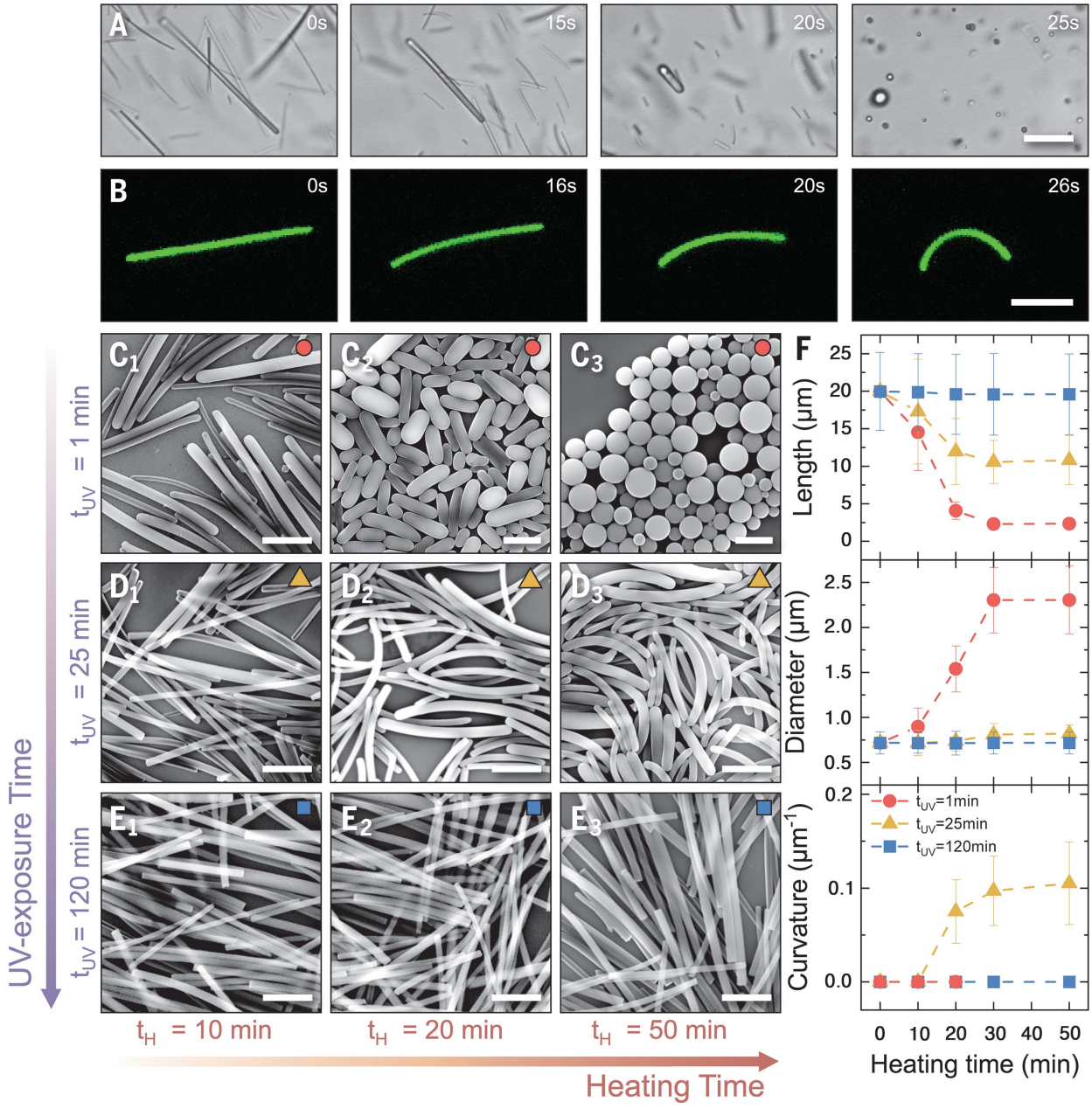

Fig. 2. Particle shape deformations during heating. (**A** and **B**) (A) Bright-field and (B) confocal microscopy snapshots of the deformation of an SU-8 rod during heating at 95°C using a heating stage; for (A), t_{UV} = 1 min, and for (B), t_{UV} = 25 min. (**C** to **E**) Representative SEM images of the shape evolution of the SU-8 rods during heating in a 95°C oven for (C) t_{UV} = 1 min, (D) t_{UV} = 25 min, and (E) t_{UV} = 120 min. (**F**) Evolution of the dimensions and curvature of the originally straight SU-8 rods during heating in a 95°C oven for t_{UV} = 1 min (circles), t_{UV} = 25 min (triangles), and t_{UV} = 120 min (squares). Error bars represent the standard deviation of the mean value. Scale bars are 10 μm in (A) and (B) and 5 μm in (C) to (E).

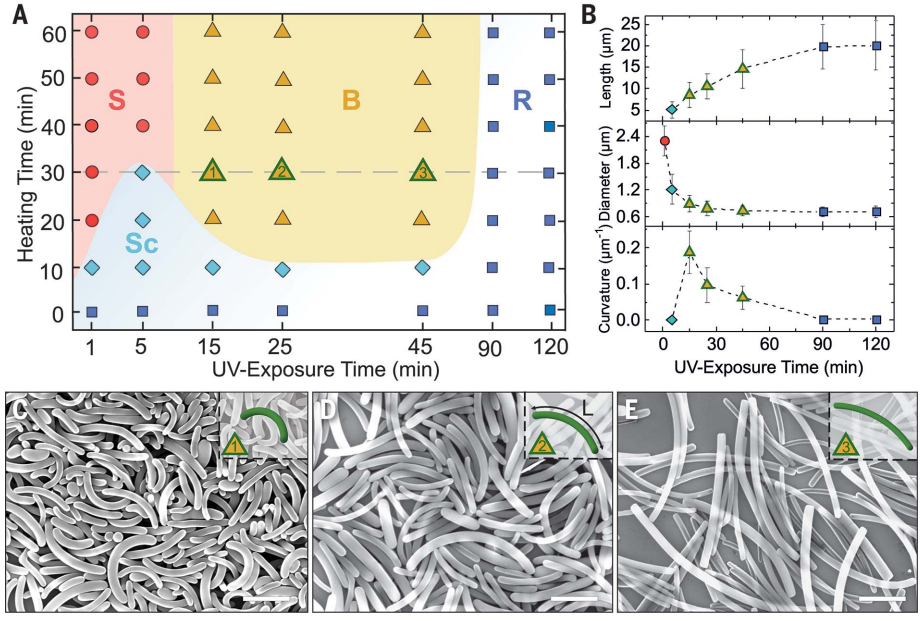

Fig. 3. Tuning particle shape and controlling the curvature and dimensions of banana-shaped particles. (**A**) Morphological state diagram of the SU-8 polymer particles as a function of UV exposure and heating times with a heating temperature of 95°C, where S, B, R, and Sc denote the sphere, banana, rod, and spherocylinder regimes, respectively. (**B**) Length, diameter, and curvature of the SU-8 particles after heating for 30 min, see dashed line in (A), in a 95°C oven for t_{UV} = 5, 15, 25, 45, 90, and 120 min. Error bars represent the standard deviation of the mean value, and the different colors of the symbols correspond to the different regimes in (A). (**C** to **E**) SEM images of banana-shaped particles with decreasing curvature obtained when t_{UV} = 15, 25, and 45 min, respectively. The insets show schematics of the bananas with their mean curvatures: (C) 0.25 μm^{-1}, (D) 0.10 μm^{-1}, and (E) 0.07 μm^{-1}. Scale bars are 5 μm.

shearing an emulsion of SU-8 droplets in a viscous medium (*29*, *30*). During the second step, the resulting rods are partially cross-linked through the ring-opening reaction of the epoxy groups under low-intensity UV light (supplementary materials section 2). The degree of cross-linking in the rods is controlled by the UV exposure time, t_{UV}, as confirmed by the infrared spectra shown in fig. S3, where the peak corresponding to the epoxy groups decreases with increasing exposure time. In the third step, the deformation into banana-shaped particles is induced by heating the rods in a 95°C oven, resulting in smoothly curved polydisperse colloidal bananas (Fig. 1, C and D; t_{UV} = 45 min). Finally, the particles are fully cross-linked by means of high-intensity UV light exposure, yielding highly stable particles that can be dispersed in both aqueous and nonaqueous solvents.

The formation of banana-shaped particles is controlled by the interplay between the cross-linking density of the SU-8 rods, tuned by the UV exposure time, and the interfacial forces induced during the heating step. The cross-linking density of SU-8 dictates its rigidity and glass transition temperature, and both increase with longer UV exposures (*31*, *32*). In our experiments, we observe three distinct responses after heating, depending on the UV exposure time. At short exposure times (t_{UV} = 1 min; Fig. 2A), i.e., low cross-linking densities, the heating of the rods results in the rounding of their sharp edges (Fig. 2C), suggesting that the rods are heated to a temperature above their glass transition temperature. The interfacial forces associated with the hemispherical particle ends drive the collapse of the rods into spheres, rather than bananas, to minimize their surface energy (*33*–*35*). This collapse takes place via a spherocylindrical intermediate state, as shown by the snapshots taken during heating in Fig. 2A (see also movie S1). From the corresponding scanning electron microscopy (SEM) images shown in Fig. 2C, we find that the particle length decreases and the diameter increases (Fig. 2F) but that the particle volume remains constant during heating (see fig. S5). At intermediate exposure times (t_{UV} = 25 min; Fig. 2B), the heating of the rods still results in the formation of round edges (Fig. 2D), which leads to an initial decrease of the rod length and an increase of the rod diameter (Fig. 2F). However, the increased cross-linking density of the rods, i.e., the higher rigidity, leads to the formation of banana-shaped particles through buckling, as directly visualized during the heating process using confocal microscopy (Fig. 2B and movie S2). The buckling manifests itself by the appearance of curvature after heating for 20 min, where the particle length and diameter no longer change considerably (Fig. 2F). At long exposure times (t_{UV} = 120 min; Fig. 2E), i.e., high cross-linking densities, no rounding of the edges is observed, suggesting that the rods are heated to temperatures below their glass transition temperature. Consequently, no shape deformation is observed, and the length, diameter, and curvature are all constant during the heating (Fig. 2F). Finally, carrying out the experiments in the dark, i.e., no cross-linking takes place, always results in the formation of spheres (fig. S4), which thus confirms the crucial role of the interplay between interfacial forces and the differing UV-induced rigidity of the rods on controlling the final particle shape.

Morphological state diagram

The ability to systematically control the final particle shape using both UV exposure and heating time (supplementary materials section 1) is summarized in the morphological state diagram shown in Fig. 3A. Within the banana regime, we show that both the dimensions and curvature of the resulting banana-shaped particles can be controlled by tuning the UV exposure time. This is observed in the SEM images presented in Fig. 3, C to E, where the bananas obtained using UV exposure times of 15, 25, and 45 min, respectively, are shown for a constant heating time of 30 min. We find that with longer UV exposure times, the mean particle length L (inset in Fig. 3D) increases from 8 to 14 μm, whereas the mean diameter and curvature decrease from 1 to 0.7 μm and from 0.25 to 0.07 μm^{-1}, respectively (Fig. 3B and fig. S6). This corroborates the fact that the rigidity of the rods increases and thus the extent of buckling decreases with UV exposure time. Inherent to the polydisperse nature of the initial SU-8 rods (*29*, *30*), the resulting colloidal bananas are also polydisperse in length, diameter, and curvature, with typical polydispersities of 30, 20, and 30%, respectively (table S1).

Phase behavior of colloidal bananas

We study the phase behavior of banana-shaped particles, and how this is affected by curvature, by preparing concentrated samples of three differently curved colloidal bananas and imaging them using confocal microscopy. Although the 3D samples are typically ~50 μm thick, we image the system relatively close to the bottom wall of

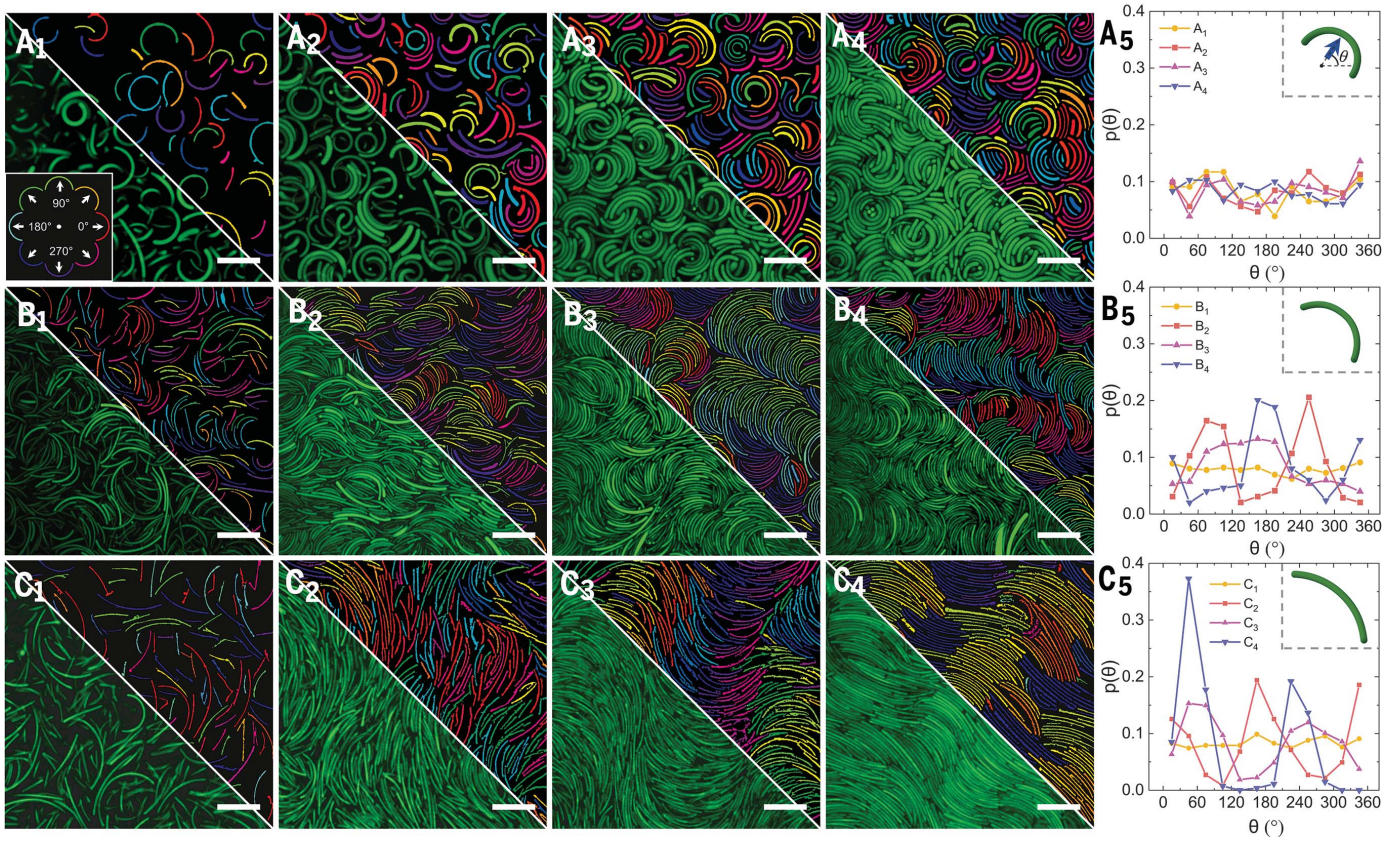

Fig. 4. Phase behavior of banana-shaped colloidal particles with different curvatures. (**A** to **C**) Confocal microscopy images of colloidal bananas with an average curvature of [(A_1) to (A_4)] $\kappa = 0.25\ \mu m^{-1}$ and packing fractions $\phi = 0.12$, 0.26, 0.61, and 0.84, respectively; [(B_1) to (B_4)] $\kappa = 0.10\ \mu m^{-1}$ and $\phi = 0.27$, 0.63, 0.79, and 0.82, respectively; and [(C_1) to (C_4)] $\kappa = 0.07\ \mu m^{-1}$ and $\phi = 0.29$, 0.60, 0.67, and 0.79, respectively. The top-right overlays on the images show the bananas colored according to their polar orientation θ as defined in the inset in (A_5) and the color legend in (A_1). (A_5), (B_5), and (C_5) show the polar angle distributions of the corresponding confocal microscopy images. The insets show schematics of the bananas with their mean curvatures. Scale bars are 10 μm.

the sample container to which the bananas align because this facilitates a quantitative 2D structural analysis at the particle level (supplementary materials section 4.2 for details). In Fig. 4, we present confocal microscopy images of the structures formed by the three differently curved colloidal bananas at different packing fractions ϕ. The most curved bananas [curvature (κ) = 0.25 μm^{-1}] only display isotropic phases (I) at all packing fractions, as shown in Fig. 4A (see fig. S9 for confocal images of the system at all packing fractions studied). Although small smectic domains are observed at high packing fractions, the combination of polydispersity and small opening angles of these bananas (table S1) suppresses the formation of any ordering at larger length scales. This is corroborated by the flat distribution of polar orientation θ (inset in Fig. 4A_5) of the bananas, $p(\theta)$, in Fig. 4A_5 and the lack of orientational correlations over space in the overlays in Fig. 4, A_1 to A_4, where the bananas are colored according to their polar orientation. Note that because of the alignment of the bananas to the wall, the orientation of the long axis is directly related to the polar orientation through a π/2 rotation (fig. S7).

The bananas with intermediate curvature, $\kappa = 0.10\ \mu m^{-1}$, also exhibit isotropic ordering at low packing fractions (Fig. 4B_1) but self-assemble into biaxial nematic and polar and antipolar smectic-like phases at higher packing fractions, as shown in Fig. 4, B_2 to B_4 (see fig. S12 for images at all packing fractions). The onset of orientational ordering in the nematic and smectic phases manifests itself as the emergence of peaks in $p(\theta)$ above $\phi = 0.63$, as shown in Fig. 4B_5. The biaxial nature of this ordering is inherent to the orthogonality of the long and polar axes of the bananas because of their alignment to the wall (see fig. S7). In particular, the biaxial nematic phase (N_b) observed at $\phi = 0.63$ (Fig. 4B_2) is characterized by two peaks in $p(\theta)$, which correspond to the two polar orientations that the bananas show in this phase. At higher packing fractions, $\phi = 0.79$ (Fig. 4B_3), the emergence of smectic domains, with some local polar smectic ordering, is observed (*36*). The polydomain structure at this packing fraction is likely due to kinetic effects (supplementary materials section 4.2) and results in a single broad peak in $p(\theta)$. Antipolar smectic ordering is observed at $\phi = 0.82$ (Fig. 4B_4), which leads to a double peak in $p(\theta)$ due to the neighboring layers exhibiting alternating polar orientation, as is also evident from the overlay in Fig. 4B_4.

Even richer phase behavior is observed for the least curved bananas ($\kappa = 0.07\ \mu m^{-1}$), as shown in Fig. 4C (see fig. S15 for images at all packing fractions). As expected, the isotropic phase is observed at low packing fractions. On increasing packing fraction, the system starts to exhibit biaxial nematic ordering (Fig. 4, C_2 and C_3), as is evident from the development of peaks in $p(\theta)$ (Fig. 4C_5), and eventually forms layered antipolar biaxial smectic structures at $\varphi = 0.79$ (Fig. 4C_4). We also observe different types of defects as shown in fig. S24. Most interestingly, however, the biaxial nematic phase of bananas with this curvature (Fig. 4C_3) exhibits a strong spatial modulation of the particle orientations,

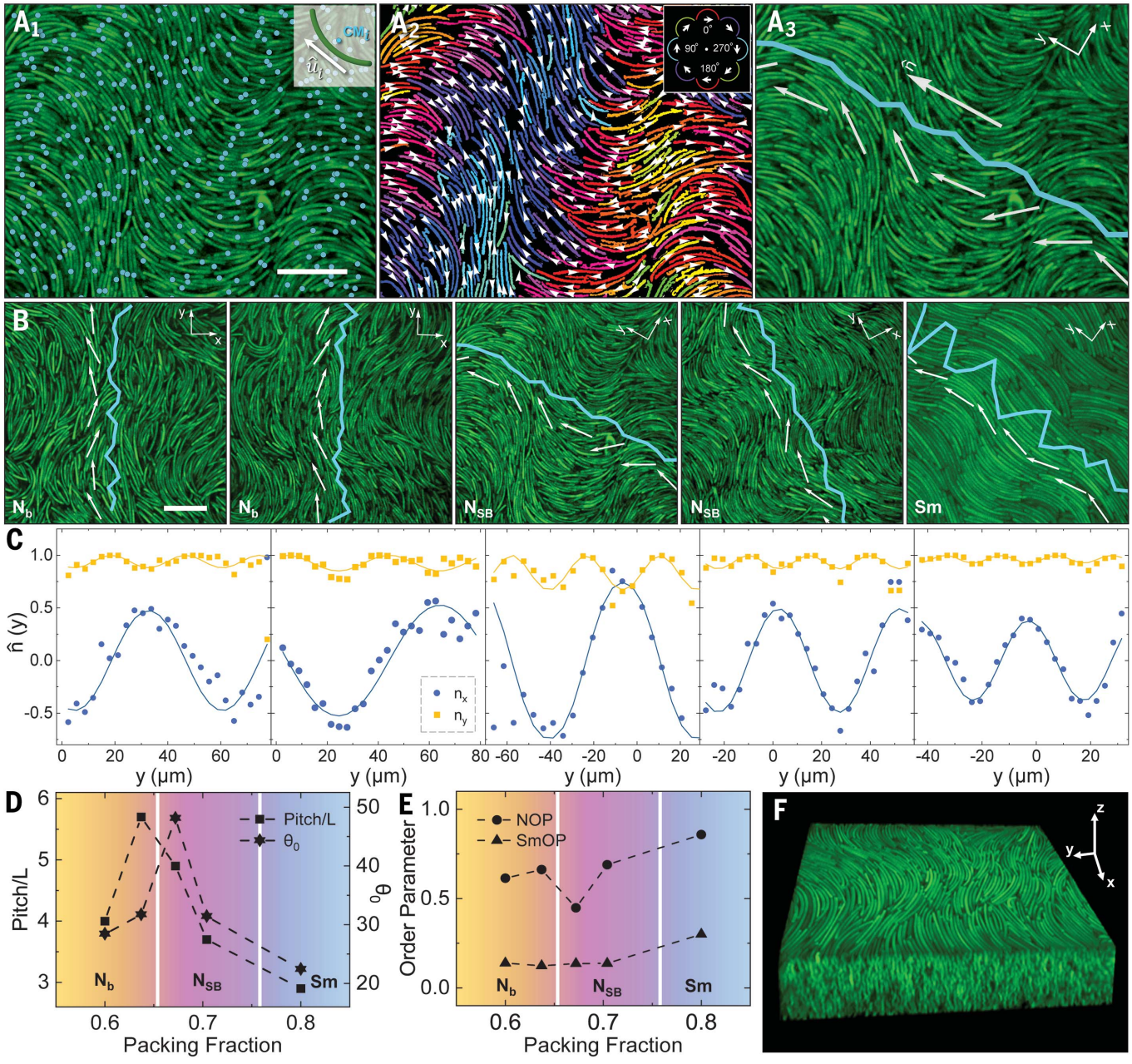

Fig. 5. Observation of the splay-bend nematic phase. (**A_1**) Center of mass (CM_i) positions of all the bananas. The inset shows a schematic of the center of mass and orientation of a banana. (**A_2**) Bananas colored according to the particle orientation as indicated by the white arrows. The inset shows the color legend used for the particle orientation. (**A_3**) The density profile $\rho(y)$ (blue line) and nematic director field $\hat{\mathbf{n}}(y)$ (white arrows) along the nematic director, $\hat{\mathbf{n}}$, of the system shown in Fig. $4C_3$. Note that the y axis is parallel to $\hat{\mathbf{n}}$. (**B**) Confocal microscopy images of the colloidal bananas with curvature $\kappa = 0.07\ \mu m^{-1}$ for packing fractions $\phi = 0.6$, 0.64, 0.67, 0.70, and 0.79, with $\rho(y)$ and $\hat{\mathbf{n}}(y)$ overlaid. (**C**) Modulation of the x and y components of the measured nematic director field along $\hat{\mathbf{n}}$. The solids lines are fits according to the theoretical expression for $\hat{\mathbf{n}}(y)$ (see main text). (**D**) Pitch-length (in units of the particle length L) and amplitude θ_0 as a function of the packing fraction. (**E**) Global nematic (NOP) and smectic (SmOP) parameters as a function of the packing fraction. (**F**) 3D confocal microscopy image (70 μm by 70 μm by 15 μm) of the splay-bend nematic phase. Scale bars are 10 μm.

which is reminiscent of the elusive biaxial splay-bend nematic phase.

Splay-bend nematic phase in colloidal bananas

To distinguish the splay-bend nematic phase from the biaxial nematic and smectic phases, we measure the spatial modulation of both the particle positions and orientations along the nematic director $\hat{\mathbf{n}}$, defined as the average particle orientation of the phase (supplementary materials section 7). To this end, we determine the center of mass positions and the particle orientations $\hat{\mathbf{u}}_\mathbf{i}$ (inset in Fig. $5A_1$) of all the particles as presented in Fig. 5, A_1 and A_2, respectively, for the least curved bananas at $\phi = 0.67$. From these, we extract the number density profile and the nematic director field along the nematic director $\hat{\mathbf{n}}$ (supplementary materials section 7), which are shown as the blue line and the white arrows in Fig. $5A_3$, respectively. Note that the y axis is defined to be parallel to $\hat{\mathbf{n}}$. In Fig. 5B, we present these measurements for the five highest packing fractions

(ϕ = 0.60 to 0.79) for the bananas with the lowest curvature (κ = 0.07 μm^{-1}). First, we observe that the number density profiles, $\rho(y)$, are mostly flat, characteristic for nematic phases, except for the highest packing fraction (ϕ = 0.79), where clear peaks develop owing to the organization of the bananas into positionally ordered smectic layers. Consistently, the global smectic order parameter (supplementary materials section 7) only increases at ϕ = 0.79, as shown in Fig. 5E, confirming the smectic nature of this phase. Second, we observe a clear modulation of the nematic director field, $\hat{\mathbf{n}}(y)$, for all five packing fractions, as is evident from the periodic fluctuations in the orientations of the white arrows in Fig. 5B.

A detailed characterization of the measured $\hat{\mathbf{n}}(y)$ is shown in Fig. 5C, where the spatial modulations of its components parallel (n_y) and perpendicular (n_x) to the nematic director are shown for all five packing fractions. To unambiguously identify the splay-bend nature of these phases, we fit the measured nematic director field with the theoretical expression for the director field of a splay-bend nematic phase (*12*), given by $\hat{\mathbf{n}}(y) = \left\{\sin\left[\theta_0 \sin\left(\frac{2\pi}{p}y\right)\right], \cos\left[\theta_0 \sin\left(\frac{2\pi}{p}y\right)\right]\right\}$, where θ_0 and p are the amplitude and pitch-length of the modulation, respectively (*12*) (fig. S18).

As shown in Fig. 5C, we find that our experimental data for n_x and n_y are notably well described by the expression for $\hat{\mathbf{n}}(y)$ for all packing fractions in the range ϕ = 0.60 to 0.79, confirming the splay-bend nature of the director field. However, for ϕ < 0.67, the amplitude θ_0 and pitch-length p, obtained from these fits, increase with increasing ϕ (Fig. 5D), in contrast to what is expected for the splay-bend nematic phase (*17*). Only for $\phi \geq 0.67$, θ_0 and p are directly proportional to each other and decrease with increasing ϕ (Fig. 5D), in agreement with computer simulations of the splay-bend nematic phase (*17*), suggesting that the splay-bend nematic phase forms at $\phi \geq 0.67$. This is corroborated by the decrease in the global nematic order parameter (supplementary materials section 7) at ϕ = 0.67, consistent with the onset of substantial splay-bend modulations of the particle orientations, resulting in a decrease of the global alignment of particles (Fig. 5E). For our least curved colloidal bananas (κ = 0.07 μm^{-1}), it is thus clear that they undergo a transition from the biaxial nematic phase to the modulated splay-bend nematic phase at $\phi \approx 0.67$, before going into the smectic phase at $\phi \simeq 0.79$. As far as we are aware, this is the first experimental observation of the splay-bend nematic phase (see also fig. S23 and movie S4), which was predicted in 1976 (*22*). Finally, we demonstrate the 3D nature of the splay-bend nematic phase in Fig. 5F, where a 3D confocal microscopy image shows the splay-bend deformations up to 15 particle diameters into the bulk of our sample (see also fig. S26).

The following picture of the phase behavior for our differently curved colloidal bananas emerges: For the most curved bananas (κ = 0.25 μm^{-1}), only the isotropic phase is observed; for the bananas with intermediate curvature (κ = 0.10 μm^{-1}), a phase sequence of I-N_b-Sm is found; and the least curved bananas (κ = 0.07 μm^{-1}) exhibit a I-N_b-N_{SB}-Sm phase sequence as a function of the packing fraction (fig. S27). The experimental observation of the splay-bend nematic phase confirms the importance of a smooth particle curvature or polydispersity for the stability of this phase (*17*) and also suggests that the typical sharp kink and purity of bent-core molecules could be one of the reasons as to why this phase has not yet been observed in molecular systems. Although our results for the least curved bananas are largely consistent with the phase behavior found in computer simulations of similar banana-shaped particles (*17*), we do not observe the N_{TB} phase, which is predicted to occur between the nematic and N_{SB} phases (*17*). We attribute the absence of the N_{TB} phase in the experimental phase behavior to a combination of the effect of gravity and the presence of a flat bottom wall in our sample cell. An external field like a gravitational or electric field may transform the N_{TB} phase into a N_{SB} phase in the case that the nematic director is perpendicular to the external field (*25*). In addition, the presence of a flat wall favors biaxial order, and hence the N_{SB} rather than the N_{TB} phase may form close to the wall. The direct observation of the colloidal analog of the N_{TB} phase therefore still remains an exciting experimental challenge.

REFERENCES AND NOTES

1. S. C. Glotzer, M. J. Solomon, *Nat. Mater.* **6**, 557–562 (2007).
2. V. N. Manoharan, *Science* **349**, 1253751 (2015).
3. A. Persat, H. A. Stone, Z. Gitai, *Nat. Commun.* **5**, 3824 (2014).
4. R. Schuech, T. Hoehfurtner, D. J. Smith, S. Humphries, *Proc. Natl. Acad. Sci. U.S.A.* **116**, 14440–14447 (2019).
5. B. Qualmann, D. Koch, M. M. Kessels, *EMBO J.* **30**, 3501–3515 (2011).
6. M. Simunovic, G. A. Voth, A. Callan-Jones, P. Bassereau, *Trends Cell Biol.* **25**, 780–792 (2015).
7. H. Takezoe, Y. Takanishi, *Jpn. J. Appl. Phys.* **45**, 597–625 (2006).
8. R. A. Reddy, C. Tschierske, *J. Mater. Chem.* **16**, 907–961 (2006).
9. A. Jákli, O. D. Lavrentovich, J. V. Selinger, *Rev. Mod. Phys.* **90**, 045004 (2018).
10. D. R. Link *et al.*, *Science* **278**, 1924–1927 (1997).
11. T. Sekine *et al.*, *J. Mater. Chem.* **7**, 1307–1309 (1997).
12. I. Dozov, *Europhys. Lett.* **56**, 247–253 (2001).
13. C. Greco, A. Ferrarini, *Phys. Rev. Lett.* **115**, 147801 (2015).
14. N. A. Clark, S. T. Lagerwall, *Appl. Phys. Lett.* **36**, 899–901 (1980).
15. F. T. Niori, T. Sekine, J. Watanabe, T. Furukawa, H. Takezoe, *J. Mater. Chem.* **6**, 1231 (1996).
16. Y. Yang *et al.*, *Sci. Adv.* **4**, eaas8829 (2018).
17. M. Chiappini, T. Drwenski, R. van Roij, M. Dijkstra, *Phys. Rev. Lett.* **123**, 068001 (2019).
18. M. Mathews, S. Kang, S. Kumar, Q. Li, *Liq. Cryst.* **38**, 31–40 (2011).
19. A. Jákli, *Liq. Cryst. Rev.* **1**, 65–82 (2013).
20. L. A. Madsen, T. J. Dingemans, M. Nakata, E. T. Samulski, *Phys. Rev. Lett.* **92**, 145505 (2004).
21. C. Tschierske, D. J. Photinos, *J. Mater. Chem.* **20**, 4263 (2010).
22. R. B. Meyer, in *Molecular Fluids*, R. Balian, G. Weill, Eds. (Gordon and Breach, 1976), pp. 271–343.
23. K. Adlem *et al.*, *Phys. Rev. E* **88**, 022503 (2013).
24. D. Chen *et al.*, *Phys. Rev. E* **89**, 022506 (2014).
25. G. Pająk, L. Longa, A. Chrzanowska, *Proc. Natl. Acad. Sci. U.S.A.* **115**, E10303–E10312 (2018).
26. F. M. van der Kooij, K. Kassapidou, H. N. W. Lekkerkerker, *Nature* **406**, 868–871 (2000).
27. Y. Yang *et al.*, *J. Am. Chem. Soc.* **138**, 68–71 (2016).
28. C. Fernández-Rico, T. Yanagishima, A. Curran, D. G. A. L. Aarts, R. P. A. Dullens, *Adv. Mater.* **31**, e1807514 (2019).
29. R. G. Alargova, K. H. Bhatt, V. N. Paunov, O. D. Velev, *Adv. Mater.* **16**, 1653–1657 (2004).
30. R. G. Alargova, V. N. Paunov, O. D. Velev, *Langmuir* **22**, 765–774 (2006).
31. R. Feng, R. J. Farris, *J. Micromech. Microeng.* **13**, 80–88 (2002).
32. K. I. Schiffmann, C. Brill, *Int. J. Mater. Res.* **98**, 397–403 (2007).
33. M. Caggioni, J. Lenis, A. V. Bayles, E. M. Furst, P. T. Spicer, *Langmuir* **31**, 8558–8565 (2015).
34. R. W. Style, A. Jagota, C.-Y. Hui, E. R. Dufresne, *Annu. Rev. Fluid Mech.* **8**, 99–118 (2016).
35. J. Bico, E. Reyssat, B. Roman, *Annu. Rev. Fluid Mech.* **50**, 629–659 (2018).
36. Y. Lansac, P. K. Maiti, N. A. Clark, M. A. Glaser, *Phys. Rev. E* **67**, 011703 (2003).

ACKNOWLEDGMENTS

We thank A. E. Stones and L. Cortes for assistance with the image analysis. **Funding:** The ERC (ERC Consolidator Grant no. 724834 – OMCIDC) is acknowledged for financial support. M.C. and M.D. acknowledge financial support from the EU H2020-MSCA-ITN-2015 project MULTIMAT (Marie Sklodowska-Curie Innovative Training Networks) (project no. 676045). **Author contributions:** C.F.-R. and R.P.A.D. conceived the project and designed the experiments. D.G.A.L.A. contributed to initiating the project and provided general expertise. C.F.-R. and H.d.S. synthesized the colloidal bananas, and T.Y. contributed to the interpretation of the synthesis mechanism. C.F.-R. performed the microscopy experiments. C.F.-R., M.C., M.D., and R.P.A.D. initiated the phase behavior study. C.F.-R. and M.C. wrote the image analysis routines and analyzed the phase behavior data. C.F.-R., M.C., T.Y., M.D., and R.P.A.D. interpreted the data. M.D. and R.P.A.D. supervised the analysis of the phase behavior. C.F.-R. and R.P.A.D. wrote the manuscript, and all co-authors commented on the manuscript. R.P.A.D. supervised the project. **Competing interests:** The authors declare no competing interests. **Data and materials availability:** All data are available in the main text or the supplementary materials.

SUPPLEMENTARY MATERIALS

science.sciencemag.org/content/369/6506/950/suppl/DC1
Materials and Methods
Figs. S1 to S27
Table S1
References (*37*–*39*)
Movies S1 to S4

25 February 2020; resubmitted 1 May 2020
Accepted 9 July 2020
10.1126/science.abb4536

Science

Shaping colloidal bananas to reveal biaxial, splay-bend nematic, and smectic phases

Carla Fernández-Rico, Massimiliano Chiappini, Taiki Yanagishima, Heidi de Sousa, Dirk G. A. L. Aarts, Marjolein Dijkstra and Roel P. A. Dullens

Science **369** (6506), 950-955.
DOI: 10.1126/science.abb4536

Controlling the curvature

Molecular chirality is often required to make chiral liquid crystalline phases, but liquid crystallinity has also been obtained using curved elongated rods known as bent-core or banana-shaped molecules. Fernández-Rico *et al.* developed a method to controllably alter the curvature of the rods using ultraviolet light and a photoresponsive polymer (see the Perspective by Godinho). From a single starting batch can come a family of rods with different curvatures but similar overall rod thickness, length, and length distribution. The researchers explored a range of liquid crystalline phases, including the splay-bend nematic phase that was predicted more than 40 years ago.

Science, this issue p. 950; see also p. 918

Science (print ISSN 0036-8075; online ISSN 1095-9203) is published by the American Association for the Advancement of Science, 1200 New York Avenue NW, Washington, DC 20005. The title *Science* is a registered trademark of AAAS.